The Composition and Structure of Ceres as Revealed by its Largest Craters.

Michael T. Bland[1], Carol A. Raymond[2], Paul M. Schenk[3], Roger R. Fu[4], Thomas Kneissl[5], Jan Hendrick Pasckert[6], Harry Hiesinger[6], Frank Preusker[7], Ryan Park[2], Simone Marchi[8], Scott D. King[9], Julie C. Castillo-Rogez[2], Chris T. Russell[10].

[1]USGS Astrogeology, Flagstaff AZ
[2]Jet Propulsion Laboratory, Pasadena CA
[3]Lunar and Planetary Institute, Houston TX
[4]Columbia University, New York, NY
[5]Institute of Geological Sciences, Freie Universität Berlin, Berlin
[6]Institut für Planetologie, Westfälische Wilhelms-Universität, Münster
[7]German Aerospace Center (DLR), Berlin
[8]Southwest Research Institute, Boulder CO
[9]Virginia Institute of Technology, Blacksburg, VA
[10]Department of Earth and Space Sciences, University of California, Los Angeles, CA

*Corresponding author: Michael Bland, USGS Astrogeology, 2255 N. Gemini Dr. Flagstaff AZ, 86001, mbland@usgs.gov, 928-556-7080.

Prior to NASA's *Dawn* mission [1], the dwarf planet Ceres was widely believed to be differentiated and contain a substantial ice-rich layer below its rocky surface [2]. At Ceres' semi-major axis (2.77 AU), its temporally averaged surface temperature virtually ensures that large impact craters should be erased on short geologic timescales if Ceres is, in fact, ice-rich [3]. In contrast to these expectations, *Dawn* Framing Camera (FC) images of Ceres revealed a heavily cratered surface [4]. Here we use digital terrain models (DTMs) derived from these images to show that most of Ceres' largest craters are several kilometers deep, suggesting little viscous relaxation of crater topography has occurred over billion year timescales. This observation, coupled with numerical simulations of viscous relaxation indicate that Ceres' subsurface must have a viscosity at least one thousand times greater than that of pure water ice. The simplest explanation is that Ceres' shallow subsurface is no more than 30%-40% ice by volume, with a mixture of rock, salts, and/or clathrates accounting for the other 60%-70%. However, a few anomalously shallow craters suggest limited viscous relaxation has occurred, possibly indicating spatial variations in the ice content of the subsurface.

Although Ceres' surface is silicate-rich [5, 6, 7], its low density (now 2163 kg m^{-3} [8]) combined with measurements of its shape (*a*-*c*) [2] previously suggested that the dwarf planet is differentiated with a rocky core overlain by a relatively pure ice layer 50-100 km thick [9]. In this model the rocky surface is likely a lag deposit representing the top of a thin (~1-10 km), mixed ice-rock layer that avoided complete melting during differentiation [10], although such a layer may be unstable to disruption by impacts and Rayleigh-Taylor overturn [9, 11]. Alternatively, Ceres' interior has been modeled as an ice-free, porous chondritic assemblage [12], although the thermal stability of such a model is uncertain [13]. The ice content of Ceres' interior has significant implications for Ceres' formation and subsequent evolution, and an ice-rich subsurface would have played a dominant role in shaping Ceres' surface morphology. Ceres is relatively warm when compared to the icy worlds of the outer Solar System (e.g., ~50-60 K warmer than Europa), with diurnally averaged equatorial temperatures of 150-160 K, mid-

latitude temperatures of ~140 K, and polar temperatures of ~120 K or less [14]. At such warm surface temperatures, ice is not strong enough to retain large-scale topography, and impact craters are expected to undergo viscous relaxation on relatively short timescales [3]. The *Dawn* mission's [1] arrival at Ceres has shown the surface to be relatively heavily cratered, including numerous craters with diameter $D \sim 100$ km [4] (Supplemental Fig. S1). The mere existence of these craters, many of which are at low latitudes (i.e., warm surface temperatures), belie predictions of a topographically "smooth", ice-rich Ceres [3]. Here we compare the depths of these largest craters with numerical simulations of viscous relaxation to constrain the physical composition of Ceres' outermost layer.

We measured the apparent depths (d_a) of Ceres' largest, clearly identifiable craters [cf. 15] using a DTM derived from *Dawn* FC images with a resolution of 140 m/pixel (from *Dawn*'s High Altitude Mapping Orbit) using stereo-photogrammetry (SPG) methods [16]. The DTM has a mean vertical error of 12 m and a horizontal resolution similar to the image resolution (140 m). Because viscous relaxation is wavelength dependent (in an infinite half space, large craters relax fastest), large craters provide the most stringent constraints on the viscosity required to maintain crater topography. We therefore focus on craters with diameters between 75 km and 280 km, and for well-preserved craters we consider our inventory complete to diameters above 80 km ($n = 25$ craters, Fig. S1). Apparent depth (i.e., depth relative to the surrounding terrain) rather than the rim depth (d_r) is used because the surrounding terrain provides the zero-potential surface to which the crater will relax (e.g., a fully relaxed crater can have $d_a = 0$, but $d_r \neq 0$). Crater depths were measured by comparing the elevation of the floor, to a characteristic elevation for the surrounding terrain (see Methods and Supplement).

Our measured crater depths are shown in Fig. 1. Ceres' topography is highly irregular over short spatial scales. The elevation of terrain surrounding each crater can therefore differ substantially in one azimuthal direction compared to another (see Supplemental material). This variability is encapsulated in the vertical bars associated with each point in Fig. 1. These bars should not be construed as formal or informal error bars. Rather each point represents the characteristic depth of each crater and the bars represent the azimuthal variability in the depth measurement.

All but one of Ceres' large craters have $d_a \geq 2$ km, and seven (Kerwan, Yalode, Urvara, Vinotonus, Zadeni, Chaminuka, and Ezinu,) have $d_a \geq 5$ km. These seven craters range in diameter from 116 km to 280 km. Many of these craters appear relatively young (Fig. S4, S5, S6, S7, S9, S11, S12, respectively); however, the crater Vinotonus (D =140 km) is superposed by numerous interior craters, including a 46-km diameter crater that has destroyed a portion of its southern rim. The relative age of Vinotonus indicates that crater topography can be maintained over long timescales. Only one crater has a characteristic apparent depth of less than 2 km: Coniraya (40° N, D = 135 km, d_a = 500 m Fig. S8). This crater is discussed in detail below. Crater depths are generally consistent with the depth of craters on Saturn's satellite Tethys [17], which has a similar surface gravity to Ceres but whose surface temperature is ~86 K. Craters on Ceres are generally deeper than those on Ganymede and Earth's Moon [18, 19].

The depths of Ceres' largest craters are not consistent with the existence of an ice-dominated layer. Figure 2 shows the measured depths of Ceres' craters compared to finite element simulations of viscous relaxation of crater topography in a pure ice layer as a function of latitude (surface temperature), crater formation time, and grain size. The simulations follow the methodology of [3] (see Methods), assume a 100-km diameter crater that is initially 4.5 km deep (based on the depths of similar sized fresh craters like Ezinu and Dantu), formation times of 1 Ga

ago and 100 Ma ago, and grain sizes of 1 mm and 10 mm [20]. Except for Kerwan, Yalode, and Urvara (D = 280, 260, and 170 km) the craters included in this investigation are within 40% of the diameter of the simulated crater. The uncertainty introduced by the use of a generic crater diameter in our simulations is not significant compared to the poorly-constrained grain size and crater formation time.

Because of the strong temperature dependence of ice rheology [e.g., 21], viscous relaxation is expected to produce distinct latitudinal variations [3]. Our measured crater depths shown in Fig. 2 demonstrate that this is not the case. Our pure-ice simulations indicate that at latitudes ≤30° (T_s ~150-160 K), viscous relaxation in a pure ice layer would result in present-day apparent crater depths of less than 500 m, even if ice grains are large (i.e., relatively high viscosity ice) and the craters formed recently (100 Ma ago). At these surface temperatures, a 100-km diameter crater can fully relax ($d_a \sim 0$) on timescales of 1-10 Ma. There are six craters with D > 75 km in this latitude band on Ceres (Fig. 2). All have a characteristic $d_a \geq 2$ km, which is much deeper than expected for a pure ice layer. The crater Dantu (D = 126 km, Fig. S10) at 24° N, for example, has d_a = 4 km. At higher latitudes (30°-50°) our simulations for a pure ice layer indicate that crater topography will still viscously relax on timescales of 10 – 100 Ma, resulting in crater depths of under 500 m for a nominal grain size of 1 mm. Craters can only retain their topography at these latitudes if the ice grains are large (10 mm, increasing the ice viscosity by a factor of ~25) and the craters formed recently. Even then present-day crater depths of just 1-2 km are expected (red curve in Fig. 2). In contrast, numerous craters with d_a exceeding 2 km are observed in this latitude range (Fig. 2). These craters include four of the five deepest on the dwarf planet: Urvara, Yalode, Vinotonus, and Ezinu.

Ceres' polar regions are cold enough to retain crater topography over long timescales even if the subsurface is pure ice. Notably, the presumably well-preserved polar craters, such as the 128-km-diameter Zadeni (70° south), have nearly equivalent depths (5 km) to similarly sized craters at lower latitudes such as the 140-km-diameter Vinotonus (43° N, 5 km depth), and the 126-km-diameter Dantu (24° north, 4 km depth). Latitudinal variations in crater depths are not observed on Ceres in the diameter (wavelength) range considered here. Latitudinal variations in topographic relaxation *were* identified on Ceres by [22], but at wavelengths generally longer than (and so more susceptible to relaxation) those investigated here.

In order to constrain the viscosity required to preserve impact crater topography, we performed numerical simulations of crater relaxation in which we systematically increase the viscosity (relative to water ice) of Ceres' subsurface. The simulated present-day depth of a 100-km diameter, 4.5-km deep crater is shown in Fig. 3 as a function of surface temperature and viscosity factor (i.e., the increase relative to pure water ice). At equatorial and mid-latitude temperatures of 150-160 K, increasing the viscosity by a factor of 100x is insufficient to retain crater topography. For these surface temperatures, only a viscosity increase of $\geq 10^3$x is sufficient to retain crater depths of greater than 2 km. At higher latitudes where surface temperatures are lower (~130 K), viscosity increases on the order of 10x are sufficient to retain topography.

An increase in the viscosity of Ceres outer shell sufficient to maintain impact crater topography for 1 Ga or longer requires the presence of a volumetrically substantial non-ice component in the subsurface. Theoretical modeling [23,24] and laboratory experiments [25, 26] indicate that particulate volume fractions (ϕ_p) of ≥ 60% are required to increase the viscosity of an ice mixture by a factor of 100x or more. Experiments in sand-ice mixtures have shown that the transition from ductile (if retarded) behavior to essentially complete immobility occurs over a very narrow range of ϕ_p (~5%) [26]. The required ϕ_p for this "jammed" behavior depends on the

distribution of grain sizes, but appears to be higher (~70%) for non-uniform grain sizes, which are likely more representative of Ceres' outer layer [26, 27]. Ceres' outer layer is therefore likely relatively ice poor, with non-ice material constituting 60-70% of the volume. This result is consistent with independent inferences of the viscosity structure of Ceres from its global shape [22].

A range of plausible compositions for Ceres' outer layer are permitted by its weakly constrained internal structure [8] and surface composition [6, 7]. That Ceres' interior is centrally condensed [8] suggests that the outer layer must have a density lower than Ceres' average density of 2163 kg m^{-3}. If Ceres' outer layer is simply a combination of silicate material (ρ_s = 2500 kg m^{-3}, likely a minimum silicate density) and ice, the 60% minimum ϕ_p required to maintain crater topography dictates a subsurface density in excess of 1800 kg m^{-3} (resulting in a relatively thick outer layer). Particulate fractions of ~70% are excluded by the density constraints if a two-component ice-silicate mixture is assumed (i.e., the resulting density is greater than Ceres' mean density). However, the addition of strong, but low-density material such as salts (hydrated or anhydrous) would have a similar effect as rock on ice rheology ([28] demonstrated this in the dislocation creep regime, and it is likely true for other flow mechanisms, though laboratory data is sparse). Low density ice clathrates are also ~100-1000x stronger than water ice at Ceres' temperatures (depending on composition and extrapolations from laboratory data taken at warmer temperatures) [29]. Salts of internal origin have been detected at Occator [30] and the occurrence of methane clathrates is predicted from geochemical models [31].The inclusion of these (or similar) low-density materials in Ceres' subsurface permits a broader range of outer layer densities (and hence, thicknesses). Ceres' subsurface is therefore more likely composed of a combination of ice, rock, and a strong, low-density material, with hydrated salts and/or clathrates likely candidates.

Despite the predominance of deep craters on Ceres, a few large craters are anomalously shallow and may provide evidence for lateral variations in the ice content of Ceres' outer layer (Fig. S3). The neighboring and similarly sized craters Coniraya and Vinotonus (both $D \approx$ 135-140 km) have vastly different apparent depths (d_a of 500 m and 5.25 km, respectively). Both craters are of similar age based on interior crater density, though counts may be near saturation (Fig. S2), and Coniraya does not appear to be obviously filled by crater ejecta from either Vinotonus or the nearby crater Gaue (ejecta from Vinotonus would have a depth of just ~250 m at the center of Coniraya assuming ejecta thickness decreases as R^{-3} [32]). Coniraya is therefore one of the best candidates for a crater on Ceres that has undergone viscous relaxation. Relaxation of a Vinotonus-like initial crater would result in Coniraya-like topography in ~1 Ga if ϕ_p is generally near the "jammed" transition but is 10-20% lower beneath Coniraya (e.g., $\phi_p \sim$ 70% beneath Vinotonus and 50-60% beneath Coniraya). This scenario is non-unique as there is a tradeoff between shorter relaxation times and lower values of ϕ_p (in the limit of $\phi_p = 0$ the relaxation time would be ~100 Ma). Alternatively, we cannot rule out the possibility that Coniraya formed from a large, very low-velocity impact that produced a similar diameter but much shallower crater than Vinotonus, but we do not favor this explanation. To first order, d/D is independent of impact velocity: the transient crater is generally parabolic so depth and diameter scale together [32].

The large, equatorial crater Kerwan is also anomalous. The crater is quite deep (5.5 km), but rather than having steep rims and a flat floor, as is typical for craters of its size, its rim is a subtle topographic step, and the crater floor gradually deepens from crater rim to center (Fig. S3). Its topography differs substantially from that of Yalode and Urvara, Ceres' next largest

craters, although unlike Vinotonus and Coniraya the age and surface temperatures of these three craters differ substantially. The morphology is consistent with viscous relaxation in a thin, low viscosity layer underlain by an immobile layer at ~30 km depth [33]. Kerwan might then provide evidence for a locally thin outer layer, an inference which may be evaluated by future *Dawn* gravity measurements. Notably, Kerwan is the largest crater on Ceres, and given its location (at the warm equator) and its size, it is the crater most expected to have undergone relaxation on Ceres. A viscously relaxed Kerwan is also consistent with observations of moderate relaxation in Ceres' equatorial region observed at long wavelengths [22].

Finally we note that the craters Kirnis (Fig. S13), Geshtin (Fig. S16), and an unnamed 100-km diameter crater at 18° N, 326° E (Fig. S14) also have relatively shallow depths that may hint at viscous relaxation; however, because their floors are geologically complex (Kirnis and Geshtin both appear to contain ejecta material from Occator (Fig. S15) and Datan, respectively, and the unnamed crater contains a large tholus) the evidence for viscous relaxation is less clear.

Viscous relaxation of Coniraya and Kerwan can likely only be achieved if the ice content (ϕ_i) in the subsurface near these craters is enhanced relative to the rest of Ceres (i.e., $\phi_i > 40\%$). However, because the transition from immobile to mobile ice-rock mixtures occurs abruptly as ϕ_i decreases [22], the corresponding variation in volume fraction may be small. The observation that most of Ceres' craters have retained their topography over long timescales, while a few craters have undergone relaxation indicates that Ceres' outer layer is geologically complex. Both the one-dimensional end-member models of [9] and [12] must therefore be abandoned in favor of interior and evolution models that predict more compositionally heterogeneous and spatially varying interior structures.

Acknowledgments:
MTB thanks Trent Hare for ArcGIS support. This work was supported by NASA's Dawn Guest Investigator program.

References:

[1] Russell, C. T., & Raymond, C. A. The Dawn mission to Vesta and Ceres. *Space Sci. Rev.* **163**, 3-23, 2011.
[2] Thomas, P. C. *et al.* Differentiation of the asteroid Ceres as revealed by its shape. *Nature* **437**, 224-226, 2005
[3] Bland, M. T. Predicted crater morphologies on Ceres: Probing internal structure and evolution. *Icarus* **226**, 510-521, 2013.
[4] Hiesinger, H. *et al*. Cratering on Ceres: Implications for its crust and evolution. *Science* submitted, 2016.
[5] Rivkin, A. S. *et al*. The surface composition of Ceres. *Space Sci. Rev.* **163**, 95-116, 2011.
[6] De Sanctis, M. C. *et al*. Ammoniated phyllosilicates with a likely outer Solar System origin on (1) Ceres. *Nature* **528**, 241-244, 2015.
[7] Ammannito, E. et al. The distribution of phyllosilicates on Ceres. *Science* submitted, 2016.
[8] Park *et al*. Interior structure of dwarf planet Ceres from measured gravity and shape. *Nature* submitted, 2016.
[9] Castillo-Rogez, J. C., & McCord, T. B. Ceres evolution and present state constrained by shaped data. *Icarus* **205**, 443-459, 2010.
[10] McCord, T. B., and Sotin C. Ceres: Evolution and current state. *J. Geophys. Res.* **110**, E05009, 2005.

[11] Roberts, J. H., & Rivkin, A. S. The fate of Ceres' original crust. *AAS Div. Planet. Sci. Conf.*, #212.07, 2015.
[12] Zolotov, M. Y. On the composition and differentiation of Ceres. *Icarus* **204**, 183-193, 2009.
[13] Castillo-Rogez, J. C. Ceres – Neither a porous nor salty ball. *Icarus* **215**, 599-602, 2011.
[14] Hayne, P. O. & Aharonson, O. Thermal stability of ice on Ceres with rough topography. *J. Geophys. Res.* **120**, 1567-1584, 2015.
[15] Marchi, S. *et al.* The missing large impact craters on Ceres. *Nature* submitted, 2016.
[16] Raymond, C. A., *et al.* The Dawn topography investigation. *Space Sci. Rev.* **163**, 487-510.
[17] White, O. L. & Schenk, P. M. Crater shapes on the Saturnian Satellites: New measurements using Cassini stereo images. *Lunar Planet Sci. Conf.* **42**, #2283, 2011.
[18] Bray, V. J., Collins, G. S., Morgan, J. V., Schenk, P. M. The effects of target properties on crater morphology: Comparison of central peak craters on the Moon and Ganymede. *Meteorit. Planet. Sci.* **43**, 1979-1992, 2008.
[19] Pike, R. J. Size-dependence in the shape of fresh impact craters on the moon. In *Impact and Explosion Cratering* (eds. Roddy, D. J., Pepin, R. O., Merill, R. B.) 489-509 (Pergamon Press, 1977).
[20] Barr, A. C. & McKinnon, W. B. Convection in ice I shells and mantles with self-consistent grain size. *J. Geophys. Res.* **112**, E02012, 2007.
[21] Durham, W. B., & Stern, L. A. Rheological properties of water ice – Applications to satellites of the outer planets. *Annu. Rev. Earth Planet. Sci.* **29**, 295-330, 2001.
[22] Fu, R. R. et al. Interior structure of the dwarf planet Ceres as revealed by surface topography. *Nature* submitted.
[23] Roscoe, R. The viscosity of suspensions of rigid spheres. *Br. J. Appl. Phys.* **3**, 267-269.
[24] Friedson, A. J., & Stevenson, D. J. Viscosity of rock-ice mixtures and applications to the evolution of the icy satellites. *Icarus* **56**, 1-14, 1983.
[25] Durham, W. B., Kirby, S. H., Stern, L. A. Effects of dispersed particulated on the rheology of water ice at planetary conditions. *J. Geophys. Res.* **97**, 20883-20897, 1992.
[26] Durham, W. B., Pathare, A. V., Stern, L. A., Lenferink, H. J. Mobility of icy sand packs, with application to Martian permafrost. *Geophys. Res. Lett.* **36**, L23203, 2009.
[27] Mangold, N., Allemand, P., Duval, P. Geraud, Y., Thomas, P. Experimental and theoretical deformation of ice-rock mixtures: Implications on rheology and ice content of Martian permafrost. *Planet. Space. Sci.* **50**, 385-401, 2002.
[28] McCarthy, C., Cooper, R. F., Goldsby, D. L., Durham, W. B., Kirby, S. H. Transient and steady state creep response of ice I and magnesium sulfate hydrate eutectic aggregates. *J. Geophys. Res.* **116**, E04007, 2011.
[29] Durham, W. B., Prieto-Ballesteros, O., Goldsby D. L., Kargel, J. S. Rheology and thermal properties of icy material. *Space Sci. Rev.* **153**, 273-298, 2010.
[30] De Sanctis, M. C. *et al.* The composition of Occator. *Nature* submitted.
[31] Castillo-Rogez, J. C. *et al.* Insights into Ceres' evolution from its surface composition.
[32] Melosh, H. J. *Impact Cratering: A Geologic Process*. Oxford University Press, New York, 1989.
[33] Parmentier, E. M. & Head, J. W. Viscous relaxation of impact craters on icy planetary surfaces: Determination of viscosity variation with depth. *Icarus* **47**, 100-111, 1981.

Methods:

We measured apparent crater depths using 16 elevation profiles for each crater, which were extracted every 22.5° and used to determine both the elevation of the crater floor and surrounding terrain (Supplemental Figs. S5-S17). The method is intentionally subjective, allowing for geologic interpretation to inform the inferred elevations, and permits a more direct assessment of the variability in crater depth as a function of azimuth. In general, the elevation of the crater floor can be determined to within a few hundred meters by this method (a few craters have substantial variation across their floors), whereas the elevation of the surrounding terrain often varies by several kilometers. These variations are reflected in the vertical bars accompanying each depth measurement shown in Fig. 1 and 2.

Simulations of viscous relaxation follow the methods described in [3]. We use the viscoelastic finite element model Tekton2.3 [34] in an axisymmetric geometry. The bottom boundary is fixed in the vertical and horizontal, and the sides of the domain are free slip in the vertical and fixed in the horizontal. The top of the domain is a free surface. The 100-km diameter crater imposed on the domain was 4.5 km deep, with a rim height of 1.4 kilometers. The floor of the crater is flat until within 20 km of the crater rim. For simplicity we do not include a central peak. The crater shape was based on Ceres' well-preserved craters Ezinu and Dantu. The simulation domain was 200 km long and 150 km deep, and had a horizontal resolution of 1 km and a vertical resolution that varied from 50 m in the near subsurface to 4 km at the base of the domain. Stresses were initialized with a combination of lithostatic stress (Ceres' surface gravity is 0.27 m s^{-2}) and topographic stress following [35].

Tekton2.3 does not explicitly include thermodynamics, but the viscosity structure of each simulation is determined by an externally calculated thermal structure, which is allowed to evolve with time. We assume Ceres' heat flux results from time-dependent radiogenic heating [3]. Thus simulations that use a crater formation time of 1 Ga ago experience both longer durations of heating, and higher maximum heat fluxes compared to simulations that assume a crater formation age of 100 Ma. However, for the timescales considered here, the change in heat flux over the course of a simulation is small. The maximum heat flux in our simulations 1 Ga ago was ~1.5 mW m^{-2}, whereas the present-day heat flux is ~1 mW m^{-2}. We examine a range of surface temperatures based on those derived for Ceres in [14].

Our simulations include all relevant flow laws for ice I, including dislocation creep (3 regimes *A*, *B*, and *C*), diffusion (*Diff*), grain-boundary sliding (*GBS)*, and basal slip (*BS*) [21]. The flow laws are combined into a composite flow law where the total strain rate $\dot{\varepsilon}_{tot}$ is given by

$$\dot{\varepsilon}_{tot} = \dot{\varepsilon}_A + \dot{\varepsilon}_B + \dot{\varepsilon}_C + \dot{\varepsilon}_{Diff} + \left[\frac{1}{\dot{\varepsilon}_{GBS}} + \frac{1}{\dot{\varepsilon}_{BS}}\right],$$

where each term on the right has the form

$$\dot{\varepsilon} = A d_i^{-m} \sigma^n \exp\left[\frac{-Q}{RT}\right],$$

and A is a rheological constant, d_i is the ice grain size, m is the grain size exponent, σ is the deviatoric stress, n is the power law exponent, Q is the activation energy, R is the gas constant, and T is the temperature. Note that we neglect the pressure dependence which is typically small. For the low stresses and warm temperatures in our simulations grain boundary sliding and diffusion dominate the rheology. Grain boundary sliding and diffusion are both grain-size-sensitive ($m \neq 0$). We nominally use a grain size of 1 mm, consistent with models of icy satellite tectonics [see discussion in 20 and 36] and terrestrial glaciers [37, 38]. We also consider larger grain sizes (10 mm) in order to insure that the retention of Ceres' topography cannot be

attributed to stiff, large-grained ice, but note that such large grains are inconsistent with the presence of particulate material, which tends to inhibit grain growth [20].

The inclusion of particulate material with ice (either hard sand [25, 26, 27] or salts [28]) is known to increase the viscosity of the mixture relative to pure samples. Based on laboratory data, the effect of particulates has been parameterized by multiplying the effective viscosity by a factor of $e^{-bn\phi_p}$, where b=2 is experimentally determined [21, 39, 3, 40]. By this formulation a particulate fraction of ϕ_p = 0.5 for grain boundary sliding (n = 1.8) results in a ~6x increase in viscosity. However, this relationship breaks down at particulate fractions above ~0.6 [24, 25, 26]. For this reason we simply increase the viscosity by a give factor (e.g., 100x or 1000x) instead of attempting to model a specific ϕ_p.

[34] Melosh, H. J. & Raefsky, A. The dynamical origin of subduction zone topography. *Geophys. J. R. Astron. Soc.* **60**, 333-334, 1980.

[35] Dombard, A. J. & McKinnon, W. B. Elastoviscoplastic relaxation of impact crater topography with application to Ganymede and Callisto. *J. Geophys. Res.* **111**, E01001, 2006.

[36] Bland, M. T. & McKinnon, W. B. Forming Europa's folds: Strain requirements for the production of large-amplitude deformation. *Icarus* **221**, 694-709, 2012

[37] De La Chappelle, S., Castelnau, O., Lipenkov, V., Duval, P. Dynamic recrystallization and texture development in ice as revealed by the study of the deep ice cores in Antarctica and Greenland. *J. Geophys. Res.* **103**, 5091-5105, 1998.

[38] Souchez, R. A., & Lorrain, R. D. *Ice Composition and Glacier Dynamics*. Springer-Verlag, Berlin, 1991.

[39] Pathare, A. V., Paige, D., Turtle, E. Viscous relaxation of craters within the martian south polar layered deposits. *Icarus* **174**, 396-418, 2005.

[40] Sori, M. M., Byrne, S., Hamilton, C. W., Landis, M. E. Viscous flow rates of icy topography on the north polar layered deposits of Mars. *Geophys. Res. Lett.* 2016.

Figures.

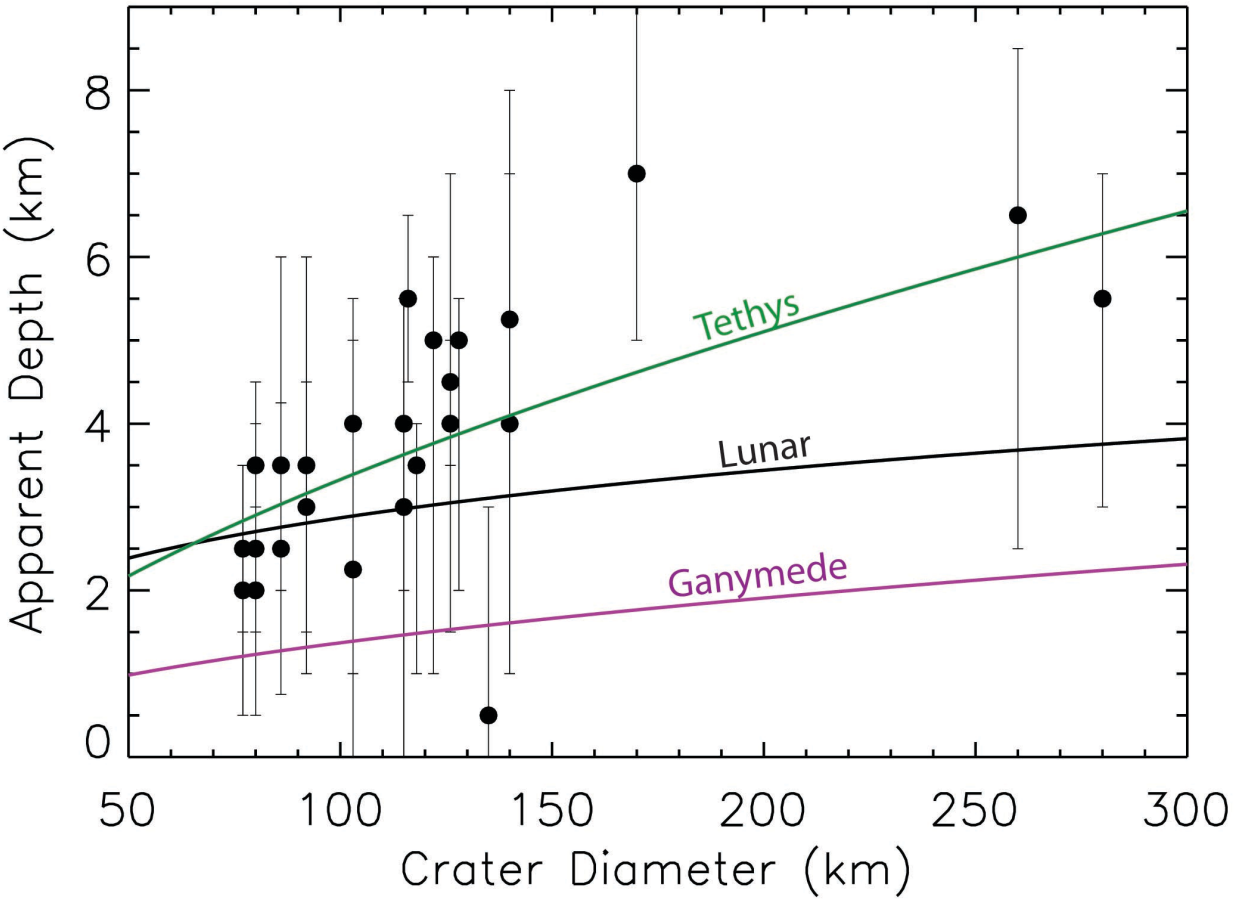

Figure 1: The apparent depths of Ceres' largest craters. Black dots indicate the characteristic depth of each crater. Vertical bars indicate the azimuthal variability of the depth due to variations in the elevation of the surrounding terrain. Curves for fresh craters on Tethys (green) [17], Ganymede (purple) [17], and the Moon (black) [18] are shown for comparison. The curves have been adjusted to account for crater rims.

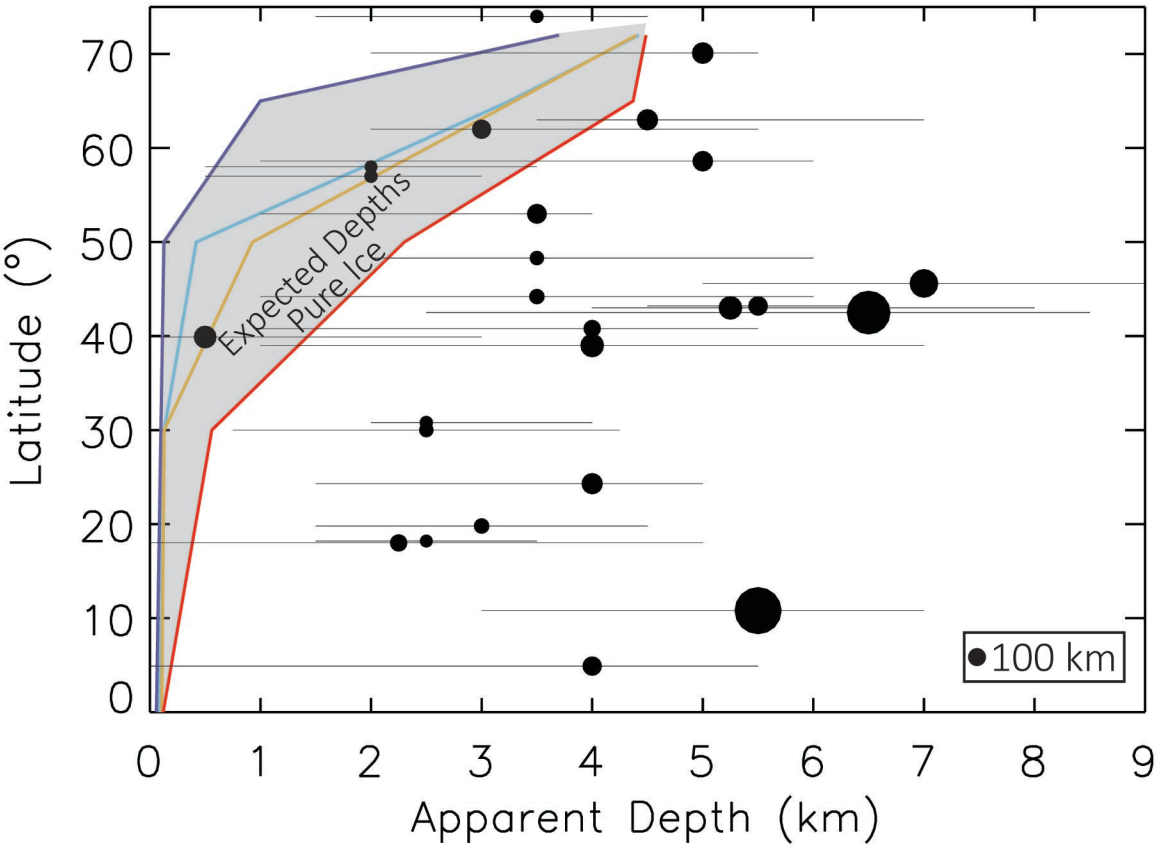

Figure 2: Comparison of the measured depths of Ceres' largest craters (black circles) with simulations of the present-day depths of 100-km craters in a pure ice layer as a function of latitude (gray region and colored lines). Line color corresponds to simulated combinations of ice grain size and crater age: 1 mm and 1 Ga (purple), 1 mm and 100 Ma (blue), 10 mm and 1 Ga (orange), and 10 mm and 100 Ma (red). Symbol size shows relative crater diameter (relative to 100 km), and the horizontal lines associated with each circle indicate azimuthal variations in crater depth.

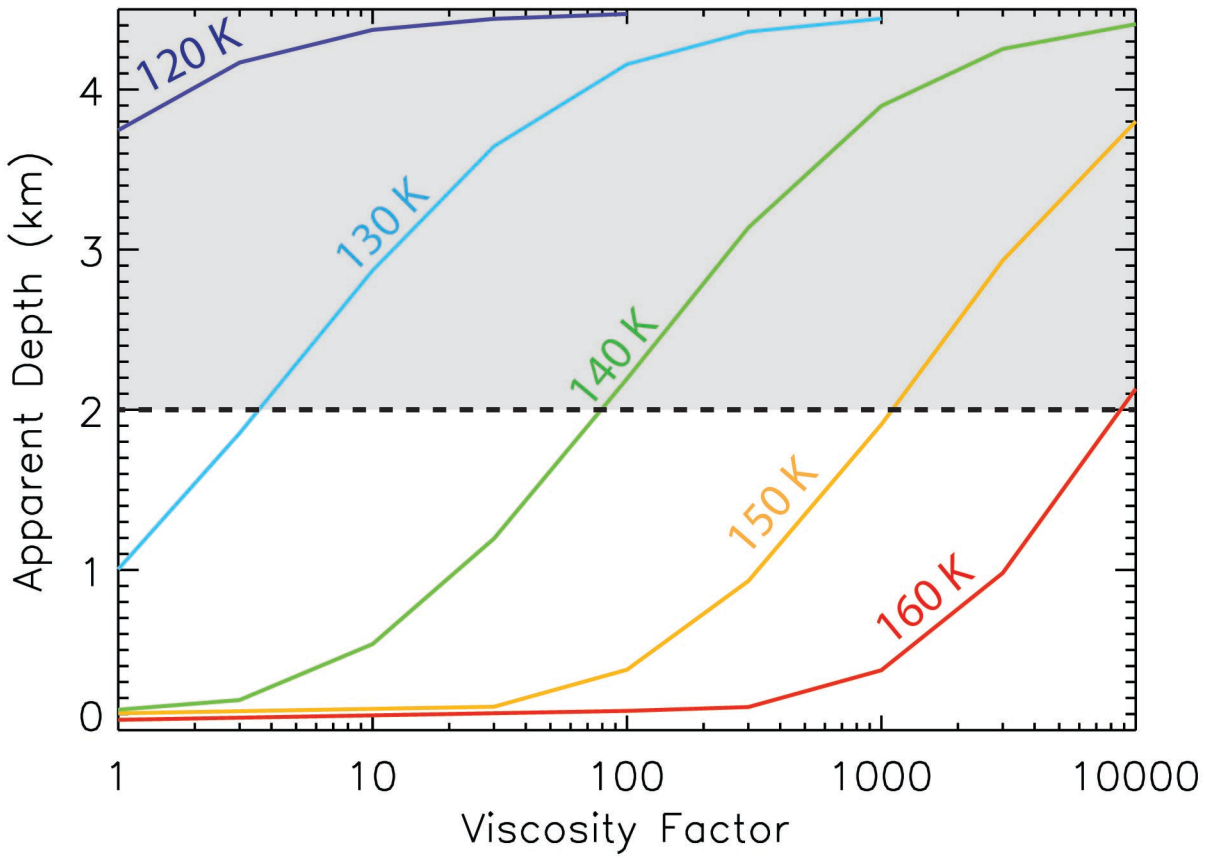

Figure 3: The simulated present-day apparent depth of a 100-km diameter crater formed 1 Ga ago that was initially 4.5-km deep as a function of viscosity increase (relative to water ice) and surface temperature. Surface temperatures (T_s) of 150-160 K correspond to latitudes < 30°, while T_s = 140 K, 130 K, and 120 K correspond to latitudes of 50°, 66°, 72°, respectively. The grey box indicates the region of typical crater depths on Ceres.

Supplemental Figures:

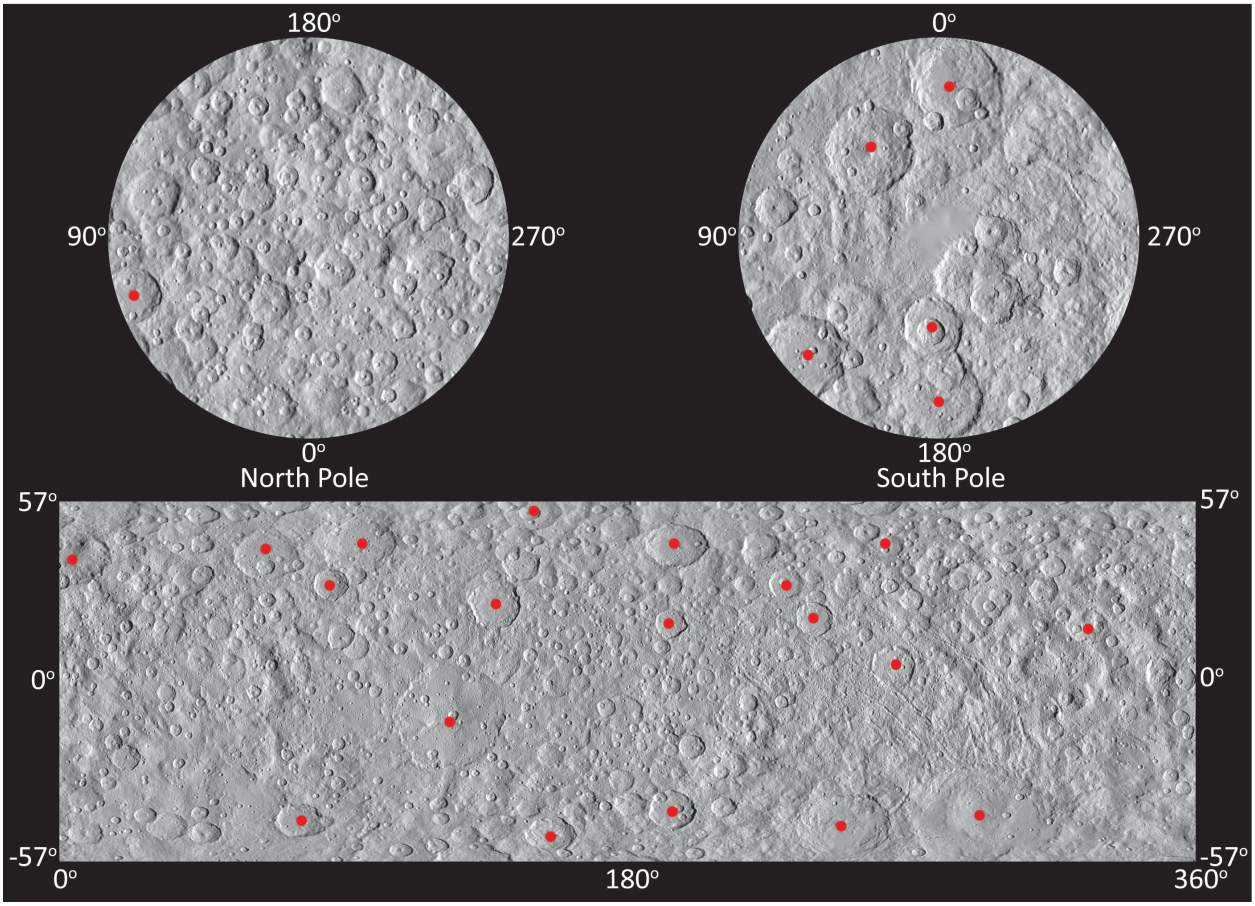

Figure S1: Shaded relief map showing locations (red dots) of the 25 craters included in this study. The shaded relief map was created from stereo-photogrammetry and has a resolution of 135 m/pixel.

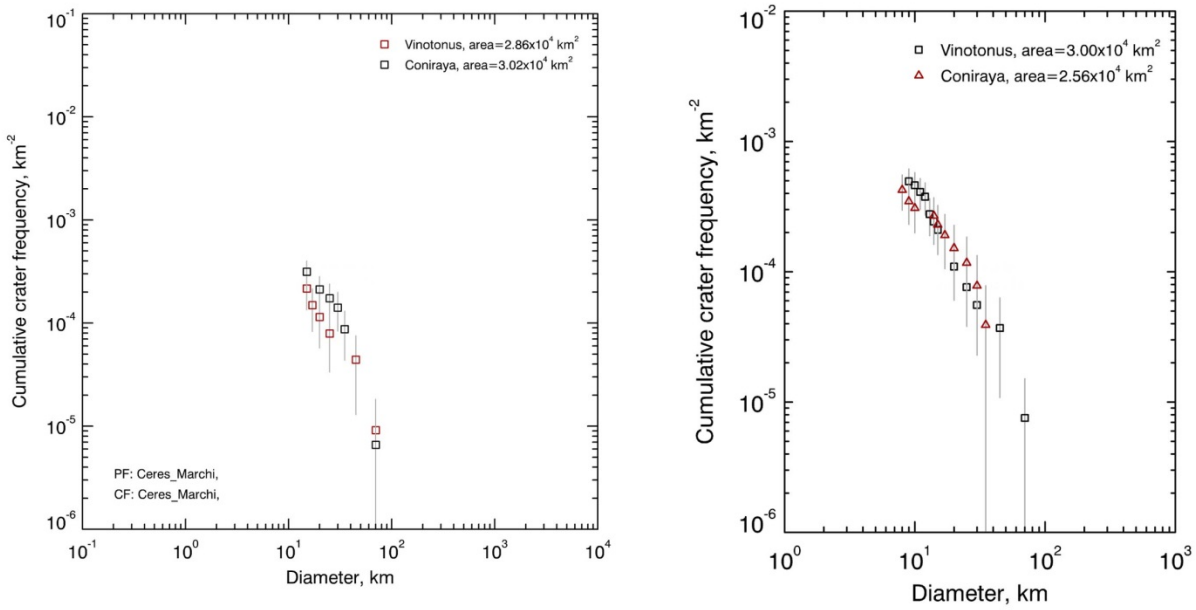

Figure S2: Two independently determined crater size frequency distributions for craters Coniraya and Vinotonus. The two craters are of similar age (error bars overlap). Both craters are heavily contaminated by secondaries and near saturation, making precise ages estimates challenging.

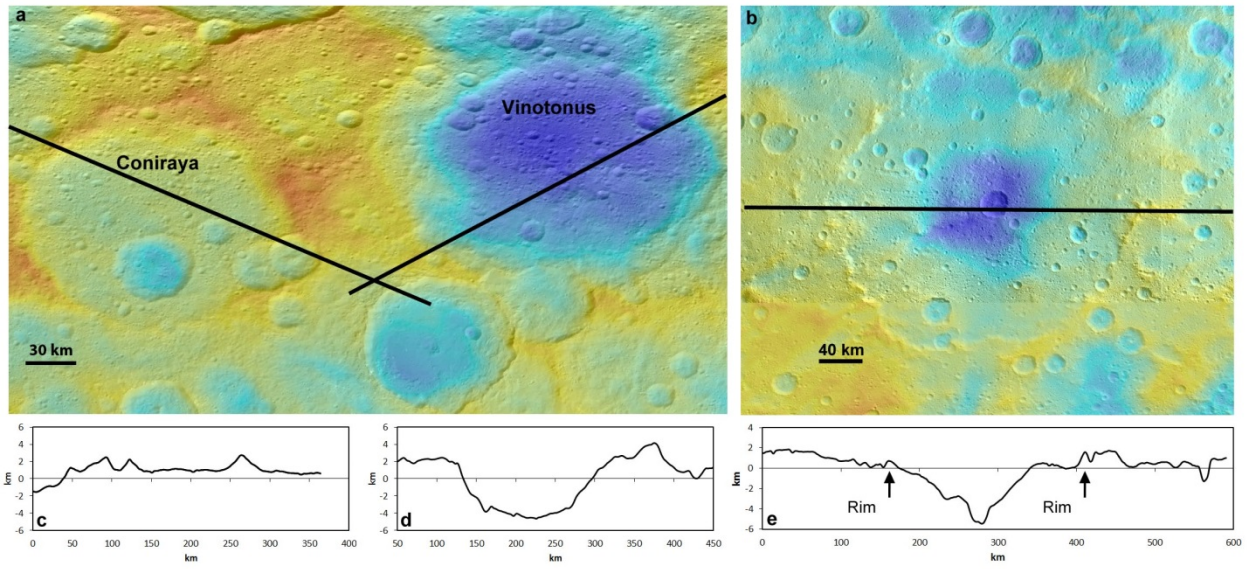

Figure S3: The topography of craters on Ceres that exhibit possible evidence for viscous relaxation. **a.** A comparison of craters Coniraya and Vinotonus. Topographic profiles (indicated by black curves in **a** and **b**) of Coniraya and Vinotonus are shown in **c** and **d**, respectively. **b.** The crater Kerwan, with an east to west profile shown in **e**. Note that the profile passes through the crater Insitor near the center of Kerwan.